Lanthanides

Deutsche Ausgabe: DOI: 10.1002/ange.201602196
Internationale Ausgabe: DOI: 10.1002/anie.201602196

Pentavalent Lanthanide Compounds: Formation and Characterization of Praseodymium(V) Oxides

Qingnan Zhang[+], Shu-Xian Hu[+], Hui Qu, Jing Su, Guanjun Wang, Jun-Bo Lu, Mohua Chen, Mingfei Zhou, and Jun Li**

Abstract: *The chemistry of lanthanides (Ln = La–Lu) is dominated by the low-valent +3 or +2 oxidation state because of the chemical inertness of the valence 4f electrons. The highest known oxidation state of the whole lanthanide series is +4 for Ce, Pr, Nd, Tb, and Dy. We report the formation of the lanthanide oxide species PrO_4 and PrO_2^+ complexes in the gas phase and in a solid noble-gas matrix. Combined infrared spectroscopic and advanced quantum chemistry studies show that these species have the unprecedented Pr^V oxidation state, thus demonstrating that the pentavalent state is viable for lanthanide elements in a suitable coordination environment.*

Oxidation state (OS) has become a central concept of chemistry and a staple of chemistry textbooks.[1] The question of just how high an OS of an element can be reached has long piqued chemists' interest.[2] The discovery of novel species with high OS helps to expand chemical understanding of the behavior of elements and their compounds. Until fairly recently, the highest observed OS had been +8, which occurs only in a few compounds including RuO_4, OsO_4, IrO_4, and XeO_4.[2–5] Recently, the IrO_4^+ cation was successfully formed in the gas phase, and was identified to contain the highest reported Ir^{IX} oxidation state.[6,7] For the light elements in each row of the main group, transition metals, and actinides, the highest OS often equals the number of available valence electrons (e.g. +3 to +6 for Al–S, Sc–Cr, and Ac–U).

However, in lanthanides (Ln) the 4f orbitals are usually extremely contracted in radial distribution and considerably lower in energy because they penetrate the [Xe] core, thus hardly participating in bonding. The chemistry of lanthanides is thus generally dominated by the low-valent +3 or +2 oxidation state despite the fact that most lanthanides have available valence 4f electrons.[8–10] Besides the omnipresent oxidation state +3, the higher oxidation state Ln^{IV} is rather common for Ce, and is encountered in Pr, Nd, Tb, and Dy as well,[10] as these lanthanides have the lowest fourth ionization energies and also the lowest +4/+3 reduction potentials.[11]

The chemistry of pentavalent lanthanides has not been explored to date.[10] A previous study presumed the presence of pentavalent praseodymium in PrO_3^- without bonding analysis.[12] However, recent density functional theory (DFT) and ab initio multiconfigurational wavefunction theory (WFT) calculations show that the Pr center in the PrO_3^- anion is in oxidation state +4 rather than the anticipated +5.[13] Herein, we report a combined experimental and theoretical study on the lanthanide oxide species PrO_4 in solid noble-gas matrix as well as the PrO_2^+ ion in the gas phase and in solid noble-gas matrix. Combined gas-phase infrared photodissociation spectroscopy, matrix-isolation infrared absorption spectroscopy, and high-level quantum chemistry studies reveal that these species have the Pr^V oxidation state.

The praseodymium oxide cation species were generated in the gas phase by using a pulsed laser vaporization/supersonic-expansion source and were studied by infrared photodissociation spectroscopy.[14–17] The mass spectra of the praseodymium oxide cations produced with O_2-seeded helium at different experimental conditions are shown in Figure 1. Spectrum (a) was obtained under experimental conditions that only those with relatively high thermodynamic stability can survive. Peaks arising from mononuclear PrO^+ and PrO_2^+ species are the most intense in the mass spectrum, thus indicating that these cations are formed preferentially with high stability. Spectrum (b) consists of progressions of peaks that can be assigned to $[(PrO)^+(O_2)_n]$ and $[(PrO_2)^+(O_2)_n]$ (n = 1–7) complexes involving strongly bound PrO^+ and PrO_2^+ core ions and weakly bound molecular O_2 ligands. Such complexes can be formed only under cold supersonic beam conditions. Enhanced abundance in the mass spectrum was found for the $[(PrO_2)^+(O_2)_n]$ cation complexes with $n = 5$ and 6. These $[(PrO_2)^+(O_2)_n]$ ($n = 5$, 6) cation complexes were selected for infrared photodissociation. Both complexes are able to dissociate by eliminating a dioxygen molecule with the dissociation efficiency increases significantly from $n = 5$ to n = 6. The infrared spectrum of $[(PrO_2)^+(O_2)_6]$ (Figure 2) shows two bands centered at 918 and 1560 cm^{-1}. The 918 cm^{-1} band is in the Pr=O stretching frequency region and is assigned to the antisymmetric OPrO stretching mode of the linear PrO_2^+ core ion. The 1560 cm^{-1} band can be attributed to the vibrations of the weakly coordinated dioxygen molecules.

In addition to the gas-phase study, the praseodymium oxide species were also prepared by the reactions of pulsed-laser-evaporated metal atoms and dioxygen in solid argon and were investigated using Fourier transform infrared absorption spectroscopy as described in detail elsewhere.[18] A previous

[*] Q. Zhang,[+] H. Qu, Dr. G. Wang, Dr. M. Chen, Prof. Dr. M. Zhou
Collaborative Innovation Center of Chemistry for Energy Materials
Department of Chemistry, Shanghai Key Laboratory of Molecular Catalysts and Innovative Materials
Fudan University, Shanghai200433 (China)
E-mail: mfzhou@fudan.edu.cn
Dr. S.-X. Hu,[+] Dr. J. Su, J.-B. Lu, Prof. Dr. J. Li
Department of Chemistry and Key Laboratory of Organic Optoelectronics & Molecular Engineering of Ministry of Education
Tsinghua University, Beijing 100084 (China)
E-mail: junli@tsinghua.edu.cn
[+] Q.Z. and S.H. contributed equally to this work.

Supporting information for this article can be found under: http://dx.doi.org/10.1002/anie.201602196.

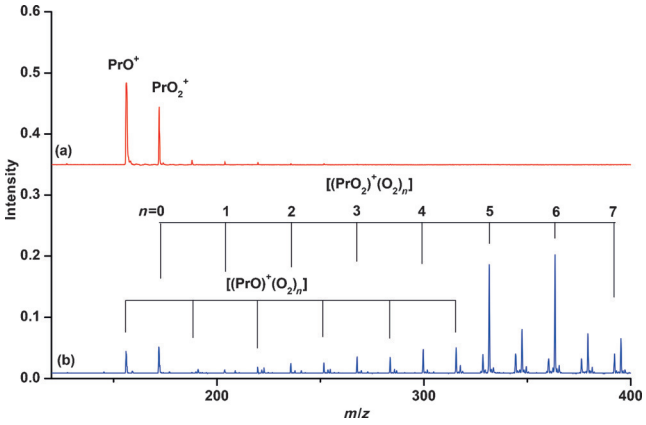

Figure 1. Mass spectra of the praseodymium oxide cationic complexes. The complexes were produced by pulsed laser vaporization of a praseodymium metal target in an expansion of helium seeded by dioxygen. Spectrum (a) was obtained from experiments with a long time delay between pulsed valve and vaporization laser, and spectrum (b) was obtained from experiments with a short time delay between pulsed valve and vaporization laser.

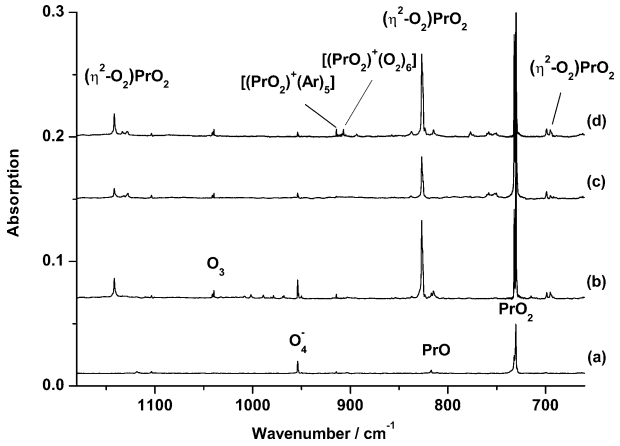

Figure 3. Infrared absorption spectra in the 1180–660 cm^{-1} region of praseodymium oxide species obtained from co-deposition of laser-evaporated Pr atoms with 0.1 % O_2 in argon. a) 1 h of sample deposition at 4 K, b) after 25 K annealing, c) after 15 min of UV light irradiation, and d) after 30 K annealing.

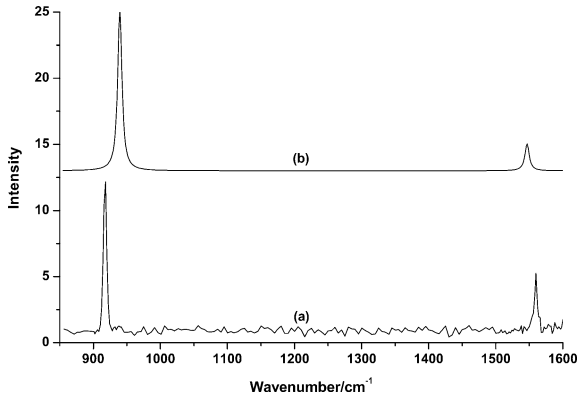

Figure 2. Experimental and simulated IR spectra of the $[(PrO_2)^+(O_2)_6]$ cationic complex. The experimental infrared photodissociation spectrum (a) is measured by monitoring the O_2 dissociation channel. The simulated spectrum (b) is obtained from the scaled (scale factor: 0.95) harmonic vibrational frequencies and intensities of the C_i structure calculated at the B3LYP level using a Lorentzian line shape with an 8 cm^{-1} full width at half-maximum.

matrix-isolation study focusing on the lanthanide mono- and dioxide species provided some preliminary indication for the formation of the PrO_2^+ species, but without addressing the bonding and oxidation state.[12] The present experiments were carried out using low O_2 concentrations (0.05–0.1 % in argon) and a relatively low laser energy to minimize the formation of multinuclear cluster species. The infrared spectra in the O–O and Pr=O stretching frequency regions from co-deposition of laser-evaporated praseodymium atoms with 0.1 % O_2 in argon are shown in Figure 3. Besides the known O_4^-, O_4^+, and O_3 absorptions that are common in the experiments on the reactions of laser-evaporated metal atoms with dioxygen,[19] the as-deposited sample exhibits three praseodymium-dependent absorption bands at 817.0, 730.3, and 914.2 cm^{-1}. These bands have previously been identified to arise from the diatomic PrO, the linear PrO_2, and PrO_2^+ (ν_3-mode) species.[12] When the sample was annealed to high temperatures (20–30 K), a group of absorptions at 1141.6, 827.0, and 695.3 cm^{-1} were formed after the PrO_2 absorption. These absorptions decreased together with the increase of the PrO_2 absorption under UV irradiation. In addition, a set of six bands at the low-frequency side of the 914.2 cm^{-1} band was produced on annealing. The lowest band in the progression (907.0 cm^{-1}) is the strongest after high-temperature annealing (See Figure S2 in the Supporting Information). The experiments were repeated under the same conditions using the $^{18}O_2$, $^{16}O_2 + {}^{18}O_2$, and $^{16}O_2 + {}^{16}O^{18}O + {}^{18}O_2$ isotopic samples to help the product identification. The isotopic spectra in selected regions are shown in Figure S3, and the product absorptions are listed in Table S1.

The 914.2 cm^{-1} band was previously attributed to the linear PrO_2^+ cation in solid argon.[12] Because of the relatively strong interaction between the cation and the argon matrix, this species should be assigned as an argon-coordinated $[(PrO_2)^+(Ar)_n]$ complex. According to our DFT calculations, the linear PrO_2^+ cation is able to coordinate five argon atoms in forming the $[(PrO_2)^+(Ar)_5]$ complex (Figure S4), which was predicted to have a D_{5h} structure with the five argon atoms coordinated equatorially to the metal center (Figure S5). Some actinide and transition-metal oxide species (including analogous UO_2^+) were previously determined to be able to coordinate five argon atoms when forming similar noble-gas complexes.[20,21] The coordinated argon atoms can be replaced by the more strongly bound dioxygen molecules on annealing. As shown in Figure S2, at the low-frequency side of the 914.2 cm^{-1} absorption, six signals at 912.9, 911.8, 910.8, 909.6, 908.3, and 907.0 cm^{-1} appeared upon sample annealing to high temperatures. These absorption signals arise from the argon–oxygen mixed $[(PrO_2)^+(Ar)_m(O_2)_n]$ complexes ($m = 1$–5, $n = 1$–6) formed by successive replacement of coordinated Ar atoms in $[(PrO_2)^+(Ar)_5]$ by molecular oxygen. The observation of six absorption signals indicates that PrO_2^+ can be coordinated by six dioxygen molecules in forming

the $[(PrO_2)^+(O_2)_6]$ complex, which is observed at 907.0 cm^{-1}. This behavior is consistent with the gas-phase value of 918 cm^{-1} determined by infrared photodissociation spectroscopy for this $[(PrO_2)^+(O_2)_6]$ complex. The observed 11 cm^{-1} gas phase-to-argon red-shift is common and arises from the matrix effect.[22] The $[(PrO_2)^+(O_2)_6]$ complex was predicted to have a C_i structure (Figure S5).

The 1141.6, 827.0, and 695.3 cm^{-1} bands are assigned to different vibrational modes of the side-on-bonded $(\eta^2\text{-}O_2)PrO_2$ molecule (Table 1), where the first two bands were attributed to this species previously.[12] The isotopic shifts and splitting clearly indicate that the 827.0 cm^{-1} band is an antisymmetric OPrO stretching mode and that the 1141.6 cm^{-1} band is an O–O stretching mode with each mode involving two equivalent O atoms. An additional weak band at 695.3 cm^{-1} showed identical behavior after irradiation and annealing. The band position and isotopic frequency ratio (1.0600) is appropriate for the symmetric OPrO stretching vibration of the $(\eta^2\text{-}O_2)PrO_2$ complex. The observed O–O stretching frequency falls in the range expected for a superoxide;[23,24] The band position of the antisymmetric OPrO stretching mode is about 100 cm^{-1} higher than that of the linear $Pr^{IV}O_2$ molecule, indicating that the two oxygen atoms in the PrO_2 fragment of $(\eta^2\text{-}O_2)PrO_2$ are both $(O)^{2-}$. Accordingly, a Pr^V oxidation state can be assigned in PrO_4, which is formed by the electron-transfer from PrO_2 to O_2.

To elucidate their structure and bonding, the praseodymium oxide species were investigated by using DFT and more sophisticated ab initio single- and multireference WFT methods: namely, the coupled-cluster method with single and double excitations and a perturbative estimate of the effect of triple excitations (CCSD(T)) and multiconfigurational methods of the complete active space self-consistent field (CASSCF), and of restricted active space (RAS) second-order perturbation theory based on RAS self-consistent orbitals (RASPT2/RASSCF), as well as density matrix renormalization group (DMRG) with huge active space (see the Supporting Information for computational details). The multiconfigurational C/RASSCF and DMRG calculations reveal that the PrO_4 and PrO_2^+ species do not have significant multireference features. Therefore, the methods of DFT and CCSD(T) are reliable for these systems, and were used to optimize the geometric structures and calculate the harmonic vibrational frequencies. The calculated CCSD T_1 values and amplitudes (Table S2) also show that there is no significant multireference feature for these species.

The neutral PrO_2 molecule is predicted to have a linear doublet ($^2\Delta_u$) ground state (Table S2). It is a Pr^{IV} species with the unpaired electron located in the metal center (Pr $4f^1$) with an electron configuration of (core) $(1\pi_g)^4\ (1\sigma_g)^2\ (2\pi_u)^4\ (2\sigma_u)^2\ (1\delta_u\text{–}4f)^1$. The PrO_2^+ cation has a linear $^1\Sigma_g^-$ ground state with a (core) $(1\pi_g)^4(1\sigma_g)^2(2\pi_u)^4(2\sigma_u)^2(1\delta_u\text{–}4f)^0$ configuration, which can be regarded as being formed by ionization of the unpaired Pr $(4f)^1$ electron of neutral PrO_2. As shown in Figure 4, the Pr–O interactions are dominated by O 2p and Pr 4f/5d orbitals. The $1\pi_g$ and $1\sigma_g$ MOs are the bonding orbitals between Pr 5d and O 2p atomic orbitals, while the $2\pi_u$ and $2\sigma_u$ MOs are weak bonding orbitals formed by Pr 4f and O 2p atomic orbitals. These wavefunction analyses clearly indicate that the Pr center has a (f^0d^0) configuration. Following the general rules for the determination of formal oxidation states, the linear PrO_2^+ cation can be classified as a Pr^V species.

Similar to the well-known uranyl ion (UO_2^{2+}), the PrO_2^+ cation prefers the linear structure to optimize the overlap of

Table 1: Observed (argon matrix) and calculated vibrational frequencies (cm^{-1}) and isotopic $^{16}O/^{18}O$ frequency ratios of PrO_2, PrO_2^+ and $(\eta^2\text{-}O_2)PrO_2$.

Species	Mode	Expt.		B3LYP		CCSD(T)
		ν	$R_{160/180}$	ν[c]	$R_{160/180}$	ν
PrO_2	as	730.3	1.0487	744.0(630)	1.0488	766.4
	ss[a]	694.2	1.0565	694.3(0)	1.0608	723.5
PrO_2^+	as			969.9(326)	1.0487	986.4
	ss			837.9(0)	1.0608	837.7
$[(PrO_2)^+(Ar)_5]$	as	914.2	1.0482	948.0(267)	1.0487	
$[(PrO_2)^+(O_2)_6]$	as	907.0 (918)[b]	1.0483	939.6(287)	1.0487	
$(\eta^2\text{-}O_2)PrO_2$	O–O	1141.6	1.0595	1145.7(195)	1.0608	1112.5
	as	827.0	1.0480	867.2(435)	1.0485	893.8
	ss	695.3	1.0600	733.4(73)	1.0608	753.8

[a] Determined from $(\nu_1+\nu_3)-\nu_3$, see the Supporting Information. as = asymmetric stretch, ss = symmetric stretch. [b] Value from gas-phase infrared photodissociation spectroscopy. [c] The B3LYP vibrational frequencies are scaled by a factor of 0.95. The IR intensities in km mol^{-1} are listed in parentheses.

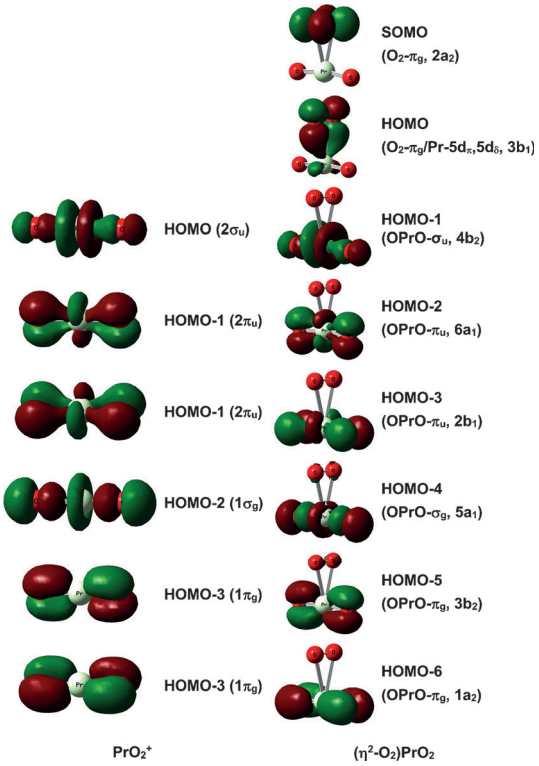

Figure 4. Frontier canonical Kohn–Sham valence MO envelopes of the linear singlet PrO_2^+ cation and the doublet $(\eta^2\text{-}O_2)PrO_2$ neutral with C_{2v} symmetry. Value of contour envelopes is 0.05 a.u.

the d and f orbitals of metal with oxygen. The Pr=O bond has a significant covalent character, with a predicted bond length of 168.8 pm at the B3LYP level or 169.9 pm at the CCSD(T) level, which is about 11 pm smaller than the sum of the triple-bond covalent radii of Pr and O reported by Pyykkö et al.[25] and is around 12 pm shorter than the Pr–O distance of neutral PrO_2 because of reduced ionic radii and increased electrostatic interaction in the cation. The calculated Mayer bond order of 2.10 is consistent with polarized-covalent Pr≡O triple-bonding interactions in PrO_2^+. Natural bond orbital (NBO) analyses confirm the Pr≡O triple bonding with two sets of localized $\sigma^2\pi^4$ bonds. The σ bond is composed of 38.4% Pr and 61.6% O character, with a Pr 5d/4f contribution of 48:50. The π bond is composed of 18.2% Pr and 81.8% O character, with a Pr 5d:4f contribution of 50:49. The significant covalent character of the Pr 5d/4f bonding in PrO_2^+ underscores the importance of the less contracted early lanthanide 5d/4f orbitals in stabilizing the high-valent oxides, which partially compensates the high fifth ionization energy for Pr^V.

The structure and bonding of the PrO_2^+ core ion in the weak van der Waals complexes $[(PrO_2)^+(Ar)_5]$ and $[(PrO_2)^+(O_2)_6]$ are essentially the same as those of the free PrO_2^+ cation. A linear $^3\Delta_g$ excited state with longer PrO bond distance is predicted to be 22.9 kJ mol^{-1} (B3LYP) or 113.0 kJ mol^{-1} (CCSD(T)) less stable than the singlet ground state (Table S2). This $^3\Delta_g$ state of the PrO_2^+ cation has a $Pr(f^1)$ configuration with an electron hole on oxygen and an oxidation state of +4. Another linear ^3H_g state with a Pr (f^2) configuration and an oxidation state of +3 is predicted to be 218.1 kJ mol^{-1} (B3LYP) or 271.3 kJ mol^{-1} (CCSD(T)) less stable than the ground state. Only the vibrational frequencies of the singlet Pr^V state match the experimental values, whereas the calculated frequencies for Pr^{IV} and Pr^{III} are much too low to match the experimental values (Table S2). These energetic and spectroscopic results show that the ground states of PrO_2^+ and its complexes all have the Pr^V oxidation state.

In addition, computational geometry optimizations were also performed on various isomers of PrO_4 with different OS and spin multiplicities, and the results are summarized in Tables S5 and S6. The lowest-energy structure is verified to be a praseodymium dioxide/superoxide complex in a doublet ground state with C_{2v} symmetry (Figure S5), consistent with the experimentally observed $(\eta^2\text{-}O_2)PrO_2$ structure. This $(\eta^2\text{-}O_2)PrO_2$ isomer lies not only lower in energy than all the other isomers with reduced OS (+2, +3, +4), but also lower in energy than the ground states of PrO_2 and O_2 reactants (13.5 kJ mol^{-1} at CCSD(T) and 45.3 kJ mol^{-1} at B3LYP), thus indicating that O_2 can oxidize PrO_2 by removing the f^1 electron to form PrO_4 with a Pr^V center. The calculated vibrational frequencies and isotopic ratios are in agreement with the experimental values (Table 1). The OPrO subunit is close to linearity (B3LYP: 170.0°, CCSD(T): 164.4°) with a bond length of around 174 pm, intermediate between that of the PrO_2^+ cation and the PrO_2 neutral molecule (Tables S2 and S6). The O_2 ligand has a typical superoxide bond length, which is loosely coordinated in the equatorial plane with a Pr–O distance of 235.8 (B3LYP) or 239.2 pm (CCSD(T)).

Bonding analysis indicates that the unpaired spin is located on the π_u^* MO of the O_2 superoxide ligand with a Pr (f^0d^0) center (Figure 4). Thus, the $(\eta^2\text{-}O_2)PrO_2$ complex can be described as $[(Pr^{+V}O_2)^+(O_2)^-]$, a neutral praseodymium oxide/superoxide species with Pr in oxidation state +5. The structure and bonding of $[(Pr^{+V}O_2)^+(O_2)^-]$ are reminiscent of those of actinide tetroxides (UO_4 and PuO_4), which were computed to be a $[(An^{+V}O_2)^+(O_2)^-]$ species as well.[26] As shown in Figures 4 and S6, the bonding between PrO_2 and O_2 is dominated by the orbital interaction between the empty d_δ and also the higher d_π orbitals of PrO_2 and the in-plane π_u^* orbital of O_2, which results in increased O–O bond length and decreased O–O stretching frequency. Population analysis indicates that the PrO_2 fragment transfers about 0.56 e$^-$ to the O_2 fragment. This charge transfer interaction strengthens the Pr=O bonds of the PrO_2 fragment and causes a blue-shift of the OPrO stretching frequency of PrO_4 with respect to that of PrO_2. We note that despite the difficulty in the assignment of oxidation states of some organometallic or lanthanide species,[27] the present assignment of Pr^V oxidation state in PrO_2^+ and PrO_4 is supported by the spectroscopic data and theoretical calculations. Lack of significant multireference features of these species also make the assignment of Pr^V less vague.

The observation of above-mentioned praseodymium oxide species in oxidation state +5 is quite surprising, especially because solid PrO_2 is an unstable material with respect to Pr_2O_3, and no pentavalent species had been observed before in solid state, solution and gas phase. However, as far as the five valence electrons are concerned, praseodymium has comparable fifth ionization energies (IE_5) to the transition-metal atoms capable of forming high OS compounds in the gas phase (IE_5 of Pr, V and Cr are 57.45, 65.23 and 69.3 eV, respectively).[28] The ionization energy of neutral PrO_2 is calculated to be only 7.4 eV at the CCSD(T) level, which is lower than some dioxide molecules such as the Group 5 and 6 species that can react with dioxygen to form stable higher-OS dioxide/superoxide complexes.[29] Apart from the relatively lower ionization potentials, the strong covalent character in PrO_2^+ and PrO_4 apparently facilitates the stabilization of the Pr^V oxidation state analogous to other well-established high-OS transition metal oxides.

To explore whether other lanthanides can also form Ln^V complexes, matrix isolation experiments were performed on the Ce, Nd, Tb, and Dy systems, which were previously reported to be able to form +4 oxidation state compounds. None of these LnO_4 species except Pr contain Ln^V oxidation state under the same conditions, which makes Pr unique in forming pentavalent neutral lanthanide species. Note that Pr has the lowest fifth ionization energy as well as the sum of the experimental first to fifth ionization energies among the whole lanthanide series (Ln = La–Lu, Table S10 and Figure S8) because of the lanthanide contraction and screening effect.

In conclusion, matrix-isolation infrared spectroscopic experiments and infrared photodissociation spectroscopic experiments with mass-selected $[(PrO_2)^+(O_2)_n]$ cations in the gas phase have shown that cationic complexes with a linear PrO_2^+ core ion and the $(\eta^2\text{-}O_2)PrO_2$ complex are

formed. The experimental observations are consistent with high-level quantum-chemical calculations showing that the PrO_2^+ cation and the $(\eta^2\text{-}O_2)PrO_2$ neutral both have a $[Xe]f^0d^0$ electron configuration for Pr. Thus, the formal oxidation state +5 for lanthanides can be assigned, which is the first report to date of an OS higher than +4 for lanthanide elements. Future macroscopic synthesis of such high-OS oxides will be interesting to obtain the crystallographic and magnetic data to validate the Pr^V oxidation state assignment in the condensed phase. This finding demonstrates that transcending the current highest oxidation state +4 for lanthanide elements is viable in an appropriate coordination environment. The existence of the pentavalent Pr in oxides points to new lanthanide chemistry involving substantial covalent bonding of the 5d/4f orbitals. New materials with such a high oxidation state may provide unique properties different from the ubiquitous di-, tri-, and tetravalent lanthanide compounds.

Acknowledgements

The work was supported by the Ministry of Science and Technology of China (2013CB834603 and 2012YQ220113-3) and the National Natural Science Foundation of China (grant nos. 21433005, 91426302, 21590792, and 21571185).

Keywords: infrared photodissociation spectroscopy · lanthanides · matrix isolation · oxidation state · praseodymium

How to cite: *Angew. Chem. Int. Ed.* **2016**, *55*, 6896–6900
Angew. Chem. **2016**, *128*, 7010–7014

[1] a) L. J. Malone, T. Dolter, *Basic Concepts of Chemistry, 8th ed.*, John Wiley & Sons, Hoboken, **2008**; b) F. A. Cotton, G. Wilkinson, C. A. Murillo, M. Bochmann, *Advanced Inorganic Chemistry*, 6th ed., Wiley-Interscience, New York, **1999**; c) N. N. Greenwood, A. Earnshaw, *Chemistry of the Elements*, *2nd ed.*, Butterworth-Heinemann, Oxford, **1997**.
[2] a) S. Riedel, M. Kaupp, *Coord. Chem. Rev.* **2009**, *253*, 606; b) S. Riedel in *Comprehensive Inorganic Chemistry II* (Eds.: J. Reedijk, K. Poeppelmeier), Elsevier, Oxford, **2013**, pp. 187–221.
[3] M. Gerken, G. J. Schrobilgen, *Inorg. Chem.* **2002**, *41*, 198.
[4] Y. Gong, M. F. Zhou, M. Kaupp, S. Riedel, *Angew. Chem. Int. Ed.* **2009**, *48*, 7879; *Angew. Chem.* **2009**, *121*, 8019.
[5] a) W. Huang, D.-H. Xing, J.-B. Lu, B. Long, W. H. E. Schwarz, J. Li, *J. Chem. Theory. Comput.* **2016**, *12*, 1525; b) W. Huang, W.-H. Xu, W. H. E. Schwarz, J. Li, *Inorg. Chem.* **2016**, DOI: 10.1021/acs.inorgchem.6b00442..
[6] G. J. Wang, M. F. Zhou, J. T. Goettel, G. G. Schrobilgen, J. Su, J. Li, T. Schlöder, S. Riedel, *Nature* **2014**, *514*, 475.
[7] a) P. Pyykkö, W. H. Xu, *Angew. Chem. Int. Ed.* **2015**, *54*, 1080; *Angew. Chem.* **2015**, *127*, 1094; b) Z. L. Xue, *Sci. China Chem.* **2015**, *58*, 4; c) P. Pyykkö, W. H. Xu, *Chem. Eur. J.* **2015**, *21*, 9468.
[8] P. B. Hitchcock, M. F. Lappert, L. Maron, A. V. Protchenko, *Angew. Chem. Int. Ed.* **2008**, *47*, 1488; *Angew. Chem.* **2008**, *120*, 1510.
[9] M. R. MacDonald, J. E. Bates, J. W. Ziller, F. Furche, W. J. Evans, *J. Am. Chem. Soc.* **2013**, *135*, 9857.
[10] a) A. Schulz, J. F. Liebman, *Struct. Chem.* **2008**, *19*, 633; b) T. Vent-Schmidt, S. Riedel, *Inorg. Chem.* **2015**, *54*, 11114; c) F. M. A. Sroor, F. T. Edelmann, Lanthanides: Tetravalent Inorganic. *Encyclopedia of Inorganic and Bioinorganic Chemistry*, Wiley, Hoboken, **2012**; d) A. F. Lucena, C. Lourenco, M. C. Michelini, P. X. Rutkowski, J. M. Carretas, N. Zorz, L. Berthon, A. Dias, M. Conceicao Oliveira, J. K. Gibson, J. Marcalo, *Phys. Chem. Chem. Phys.* **2015**, *17*, 9942.
[11] S. G. Bratsch, J. J. Lagowski, *J. Phys. Chem.* **1985**, *89*, 3317.
[12] S. P. Willson, L. Andrews, *J. Phys. Chem. A* **1999**, *103*, 3171.
[13] J. Su, S.-X. Hu, W. Huang, M. F. Zhou, J. Li, *Sci. China Chem.* **2016**, *59*, 442.
[14] a) M. A. Duncan, *Int. Rev. Phys. Chem.* **2003**, *22*, 407; b) A. M. Ricks, Z. E. Reed, M. A. Duncan, *J. Mol. Spectrosc.* **2011**, *266*, 63.
[15] a) M. Okumura, L. I. Yeh, J. D. Myers, Y. T. Lee, *J. Chem. Phys.* **1986**, *85*, 2328; b) M. Okumura, L. I. Yeh, J. D. Myers, Y. T. Lee, *J. Phys. Chem.* **1990**, *94*, 3416.
[16] a) W. H. Robertson, M. A. Johnson, *Annu. Rev. Phys. Chem.* **2003**, *54*, 173; b) T. Ebata, A. Fujii, N. Mikami, *Int. Rev. Phys. Chem.* **1998**, *17*, 331; c) E. J. Bieske, O. Dopfer, *Chem. Rev.* **2000**, *100*, 3963.
[17] a) G. J. Wang, C. X. Chi, X. P. Xing, C. F. Ding, M. F. Zhou, *Sci. China Chem.* **2014**, *57*, 172; b) G. J. Wang, C. X. Chi, J. M. Cui, X. P. Xing, M. F. Zhou, *J. Phys. Chem. A* **2012**, *116*, 2484.
[18] G. J. Wang, M. F. Zhou, *Int. Rev. Phys. Chem.* **2008**, *27*, 1.
[19] a) G. V. Chertihin, L. Andrews, *J. Chem. Phys.* **1998**, *108*, 6404; b) M. F. Zhou, J. Hacaloglu, L. Andrews, *J. Chem. Phys.* **1999**, *110*, 9450.
[20] a) J. Li, B. E. Bursten, B. Liang, L. Andrews, *Science* **2002**, *295*, 2242; b) L. Andrews, B. Y. Liang, J. Li, B. E. Bursten, *J. Am. Chem. Soc.* **2003**, *125*, 3126; c) X. F. Wang, L. Andrews, J. Li, B. E. Bursten, *Angew. Chem. Int. Ed.* **2004**, *43*, 2554; *Angew. Chem.* **2004**, *116*, 2608; d) J. Li, B. E. Bursten, L. Andrews, C. J. Marsden, *J. Am. Chem. Soc.* **2004**, *126*, 3424.
[21] a) Y. Y. Zhao, G. J. Wang, M. H. Chen, M. F. Zhou, *J. Phys. Chem. A* **2005**, *109*, 6621; b) Y. Y. Zhao, Y. Gong, M. H. Chen, C. F. Ding, M. F. Zhou, *J. Phys. Chem. A* **2005**, *109*, 11765; c) Y. Y. Zhao, M. F. Zhou, *Sci. China Chem.* **2010**, *53*, 327.
[22] M. E. Jacox, *Chem. Soc. Rev.* **2002**, *31*, 108.
[23] C. J. Cramer, W. B. Tolman, K. H. Theopold, A. L. Rheingold, *Proc. Natl. Acad. Sci. USA* **2003**, *100*, 3635.
[24] Y. Gong, M. F. Zhou, L. Andrews, *Chem. Rev.* **2009**, *109*, 6765.
[25] P. Pyykkö, S. Riedel, M. Patzschke, *Chem. Eur. J.* **2005**, *11*, 3511.
[26] a) W. Huang, W. H. Xu, J. Su, W. H. E. Schwarz, J. Li, *Inorg. Chem.* **2013**, *52*, 14237; b) W. Huang, P. Pyykkö, J. Li, *Inorg. Chem.* **2015**, *54*, 8825; c) J. Su, W. L. Li, G. V. Lopez, T. Jian, G. J. Cao, W. L. Li, W. H. E. Schwarz, L. S. Wang, J. Li, *J. Phys. Chem. A* **2016**, *120*, 1084.
[27] A. Kerridge, R. Coates, N. Kaltsoyannis, *J. Phys. Chem. A* **2009**, *113*, 2896.
[28] R. C. Weast, *CRC Handbook of Chemistry and Physics*, *63rd ed.*, CRC, Boca Raton, **1982**.
[29] a) M. F. Zhou, L. Andrews, *J. Phys. Chem. A* **1998**, *102*, 8251; b) Y. Y. Zhao, Y. Gong, M. H. Chen, M. F. Zhou, *J. Phys. Chem. A* **2006**, *110*, 1845; c) Y. Y. Zhao, J. Su, Y. Gong, J. Li, M. F. Zhou, *J. Phys. Chem. A* **2008**, *112*, 8606; d) M. F. Zhou, L. Andrews, *J. Chem. Phys.* **1999**, *111*, 4230.

Received: March 3, 2016
Published online: April 21, 2016

